Desalination and Water Treatment
www.deswater.com
doi: 10.5004/dwt.2021.27397

229 (2021) 69–78
July

Development of polybenzimidazole ultrafiltration hollow-fiber membranes

Xiao Wang[a], Khaled bin Bandar[b], Michael D. Wales[a,*], Palitha Jayaweera[a], Radwan A. Alrasheed[b], Saad A. Aljlil[b], Indira Jayaweera[a]

[a]*SRI International, 333 Ravenswood Avenue, Menlo Park, CA 94025, USA, Tel. +1-650-859-3169; emails: michael.wales@sri.com (M.D. Wales), xiao.wang.chem@gmail.com (X. Wang), palitha.jayaweera@sri.com (P. Jayaweera), indira.jayaweera@sri.com (I. Jayaweera)*
[b]*National Center for Water Treatment and Desalination Technology, King Abdulaziz City for Science and Technology, P.O. Box: 6086, Riyadh 11442, Saudi Arabia, emails: kbandar@kacst.edu.sa (K.b. Bandar), alrasheed@kacst.edu.sa (R.A. Alrasheed), saljlil@kacst.edu.sa (S.A. Aljlil)*

Received 14 January 2021; Accepted 3 May 2021

ABSTRACT

Polybenzimidazole (PBI) ultrafiltration (UF) hollow-fiber membranes (HFMs) were fabricated using a continuous fiber-spinning line developed at SRI International. Based on the previously developed fabricating conditions for reverse osmosis (RO) and nanofiltration (NF) HFMs, UF HFMs with a large open pore size (50–100 nm) at the shell barrier layer were obtained by switching the dry-jet wet-spinning process to a complete wet-spinning process. To maximize the membrane permeability, bore solution compositions were formulated based on the previous composition, and 100% isopropanol was noticed leading to the largest open pore size on the lumen side. The flow rate ratio of solutions was adjusted during fiber spinning to reduce the fiber wall thickness and the optimized wall thickness, 95 μm was obtained to sustain a running at 20 psi when the flow rates of bore solution and dope solution were 0.35 and 0.9 mL/min, respectively. With the above optimal fabricating protocol, a PBI UF HFM with a pure water flux of 58 LMH at 20 psi was fabricated and its pore size was measured to be 21–25 nm by capillary flow porometry. The resulting UF HFMs showed a good anti-fouling performance in a series of filtration tests with humic acid, bentonite clay, and bovine serum albumin as foulants.

Keywords: Polybenzimidazole; Ultrafiltration; Hollow-fiber membrane; Air gap; Fouling

1. Introduction

Chemical separations consume roughly half of all industrial energy usage in the United States and about 15% of country's total energy usage [1]. Membrane separation is a preferred filtration method in the water, energy, chemical, petro-chemical, and pharmaceutical industries. Defect-free membranes are highly efficient, can be produced at a large scale, and have high fiber-packing density volume ratios [2]. Flat-sheet, membrane-based, and spiral-wound modules currently dominate the market because they are comparatively inexpensive; however, cartridges consisting of hollow-fiber membranes (HFMs) have great potential for commercialization because of their self-supporting structure, high fiber-packing density [3], and large surface area per unit of module space (around one order of magnitude higher than spiral-wound modules [4]). To further enhance surface area and filtration efficiency, SRI developed a continuous

* Corresponding author.

production line and a corresponding spinning technology to fabricate high-performance, ultra-fine HFMs (OD < 500 μm) [5,6]. The HFM is based on an advanced polymeric material, polybenzimidazole (PBI), which has a high continuous operating temperature (as high as 250°C) [7], robust mechanical stability [8], and outstanding chemical resistance [9].

A previous study conducted by SRI International indicated PBI HFMs provided filtration performance comparable to that of commercial reverse osmosis (RO) and nanofiltration (NF) products [5]. The flux and selectivity of the PBI HFM barrier layer can be tuned by merely varying the air gap between the spinneret and coagulation bath. When the air gas is <1.27 cm (0.5 inch), the HFM exhibits a selectivity close to ultrafiltration (UF) but a water flux inferior to UF. UF membranes are widely used to effectively remove suspended particles, turbidity, bacteria, colloids, algae, parasites, and viruses, clarification, and disinfection purposes and have a prevalent application in water treatment and biotechnology [10–13]. The current commercial UF HFMs are mainly based on polyvinyl chloride, polysulfone, polyvinylidene fluoride, and cellulose acetate [14]. The successful development of PBI UF HFMs will provide more alternatives for UF application and leverage the SRI technology to spin a series of HFMs (for gas separation, RO, NF, and UF) using the same production line and same dope formulation with only slight differences in spinning conditions. Application of PBI HFMs has been studied for gas separations [15–17], RO [5,18,19], and NF [5,20]. To the best of our knowledge, there are no publications describing PBI UF HFMs.

The PBI HFMs are fabricated by a dry–wet spinning process, in which a delayed demixing leads to a sponge-like sublayer beneath a dense barrier layer [21]. In the asymmetric outside-in configuration, water permeability is affected by both the dense barrier layer and sublayer. Therefore, we varied spinning conditions to enhance the permeability of PBI UF HFMs and observed that the pore size was reversely related to the air gap; we then used wet spinning (0 cm air gap) to explore how we could achieve the maximum barrier layer pore size. We formulated the bore solution composition to optimize the open pore size of the inner sublayer, and we adjusted the flow rate ratio of the bore and dope solutions to control the entire membrane thickness (i.e., wall thickness). The coagulation bath composition was tuned to introduce more macro-voids in the sublayer and lower the resistance to water flow. Moreover, we applied three different foulants (i.e., humic acid (HA), bentonite, and bovine serum albumin (BSA)) to assess the separation performance of the newly developed PBI UF HFMs and their antifouling capabilities.

2. Experimental

2.1. Materials and reagents

Isopropyl alcohol (IPA), methanol (MeOH), and dimethylacetamide (DMAc) were purchased from Macron Fine Chemicals (United States). Glycerol (Gly) was purchased from Alfa Aesar Chemicals (United States). The PBI used in this experiment is poly[2,20-(m-phenylen)-5,5′-bisbenzimidazole], and its chemical structure is shown in Fig. 1. The PBI dope solution containing DMAc, polyvinylpyrrolidone (PVP), and IPA was supplied by PBI Performance Products Inc. (United States), and used for HFM spinning. The bore solution was a mixture of nonsolvents including methanol (MeOH), IPA, and Gly. A coagulation bath consisting of MeOH and IPA were used to form an outer dense layer of PBI HFM through phase inversion. The HA, BSA, bentonite clay, and sodium dodecyl sulfate (SDS) were purchased from Sigma-Aldrich (United States).

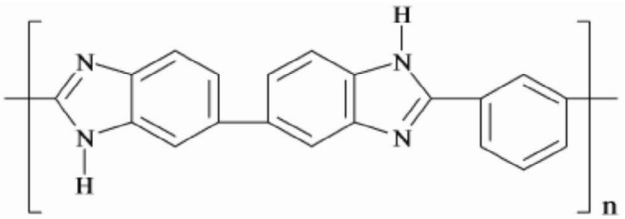

Fig. 1. Chemical structure of poly[2,20–(m-phenylen)-5,5′-bisbenzimidazole] (PBI).

2.2. Fabrication of PBI HFMs and preparation of fiber module

The configuration of the continuous production line at SRI and the fabrication process for the PBI HFMs are detailed in previous publications [5,22]. The PBI dope solution (with a viscosity of 19,000–21,000 cP) was extruded using a syringe pump (1,000 D, Teledyne ISCO, Lincoln, NE, USA) from a spinneret at 35°C–55°C and a flow rate of 0.9–2.0 mL/min. The same dope formulation was used for all experiments, and is the same formulation used in previous publications [5]. We maintained the HFM lumen using a bore solution (mixture of nonsolvent alcohols) and a flow rate of 0.2–1 mL/min; although several bore solutions were tested (Section 3.1.2. Optimization of lumen open pore size) IPA was settled on. The asymmetric membrane structure was formed in a coagulation bath containing MeOH and IPA at 5°C–15°C followed by water wash at ambient temperature to further the phase inversion. The HFMs were collected on a take-up drum and washed in a warm water bath to remove chemical residuals. The range of the various parameters tested are listed in Table 1, as well as the final spinning values. The PBI HFM modules were prepared by epoxying 50 fibers (28 cm long) following the regular shell feed design [4]; the resulting effective area of each module was approximately 245 cm^2.

2.3. Scanning electron microscopy measurements

The PBI HFMs were chilled and fractured in liquid nitrogen for cross-section observation. All the samples were coated by platinum sputtering and observed using a field-emission scanning electron microscopy (FE-SEM) (JEOL6700, JEOL Ltd., Peabody, MA, USA) in a lower secondary electron (LEI) mode with an accelerating voltage of 3 KV and a probe current of 20 μA.

2.4. Capillary flow porometry

Pore size distribution of PBI HFMs were measured by a 3Gwin porometer at Anton Paar (United States). The test

condition and data analysis are detailed in the test report submitted as a Supplementary Material.

2.5. Membrane filtration tests

The HA feed solution was prepared by 100-fold dilution of 5 g/L HA stock solution. The pH values of the feeds were adjusted to 4, 7, and 9.5, respectively, using 1 M NaOH or 1 M HCl. The bentonite feed was prepared by stirring a 10 g/L suspension for 24 h at 300 rpm followed by a further 30 min stirring at 40 rpm. The resulting bentonite suspension was allowed to stand overnight, and the supernatant was collected as a stock solution. The stock solution for the feed was diluted to turbidity of 70 NTU. A 10 g/L BSA stock solution was prepared in a 0.5 M phosphate buffer (pH = 7.4); the BSA feed solution was made by diluting the stock solution to 1,500–1,600 ppm. The solution concentrations of HA [23], bentonite [24,25], and BSA [26] were determined according to the published previous study.

We began all filtration tests by measuring the pure water flux. The sample modules were compacted in deionized (DI) water under 40 psi at room temperature, and the flux was measured at 20 psi with a feed flow rate of 8 L/min. The permeate was collected in a beaker and weighed in a top-loading balance. The permeate weight variation was recorded every 10 min. Water flux was calculated by normalizing the flow rate with the effective surface areas and reported as L/(m^2 h) (LMH). Then, the solid content (oil/water, HA, BSA, and bentonite) was introduced for the antifouling test. The rejection percentage (%Rejection) was determined by the following equation:

$$\%\text{Rejection} = \left[1 - \frac{C_p}{C_f}\right] \times 100 \quad (1)$$

where C_p is the permeate concentration and C_f is the feed concentration. For HA and BSA, the absorbance (A) ratio was measured using a UV-vis spectrometer (HP Agilent 8453, United States) at 254 and 280 nm, respectively, so that we could calculate C_p/C_f according to Beer's Law. The calibration curve for BSA consists of 5 points, ranging from 30 to 4,500 ppm, with an R^2 of 0.999. The calibration for HA consists of 5 points ranging from 1.2 to 152 ppm, with an R^2 is 0.999. Calibration curves for BSA and HA are provided in the Supplemental material. For the bentonite suspension, the nephelometric turbidity unit (NTU) was measured by a turbidity meter (Sper Scientific 860040, United States). The NTU ratio was obtained for C_p/C_f because NTU is linearly proportional to the suspended sediment concentration [27].

In the custom-built UF system (Fig. 2), the feed solution in the reservoir was pumped through HFMs via a diaphragm pump, and the retentate solution was sent back to the reservoir for further recirculation. The hydraulic pressure in the HFM module was monitored by a pressure gauge on the feed side, and we adjusted it using a pressure-control valve on the retentate side. We used a flow monitor to assess the feed flow rate and tuned it with a hydraulic control valve next to the pump outlet. For all filtrations tests, the foulant was applied to the shell-side, and the filtered water permeated through the bore-side.

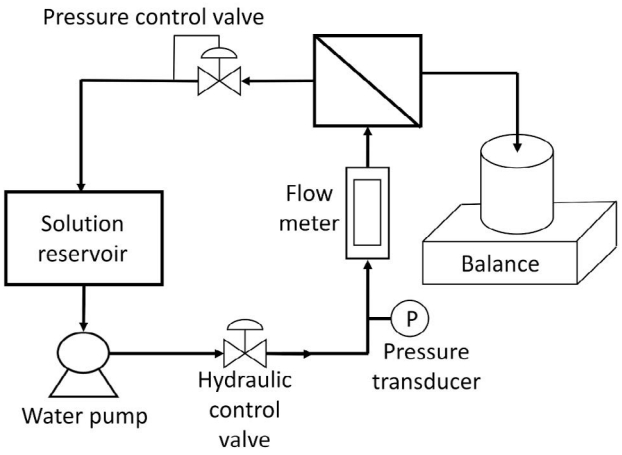

Fig. 2. Schematic diagram of UF test system.

3. Results and discussion

3.1. Optmization of fiber morphology for a PBI UF HFM

A typical outside-in polymeric HFM structure consists of four types of morphologies: asymmetric outer selective skin layers, finger-like macrovoids, sponge-like substructures, and porous inner skin layers [28]. An ideal high-performance HFM should have: (1) a large enough average pore size and porosity at the shell side to allow suitable selectivity and high permeability; (2) a sublayer with a high porosity; (3) an appropriate ratio of finger-like macrovoids to further reduce water flow resistance; (4) a large average open pore size on the lumen side, and (5) a thin wall. Therefore, the following experiments were conducted to optimize the fabricating conditions of PBI UF HFMs step by step.

3.1.1. Optimization of barrier layer pore size

A previous study by our group indicated air gap was a key factor in determining HFM barrier layer pore size, and we tuned the pore size from poreless to UF scale when the air gap varied from 4 inch (10.16 cm) to 0.5 inch (1.27 cm) [5]. However, the low water permeability of the resulting UF HFM (slightly higher than PBI NF HFMs) limited its commercial application and exploration of new fabricating conditions is necessary. According to Chung and Hu [29], the HFM barrier layer is formed by two steps during the dry-jet, wet-spinning process. A slow, ambient moisture-induced precipitation occurs in the extruded nascent fiber shell to slow down the solvent exchange and polymer chain contraction in the coagulation bath so the contracting polymer chains in HFM shell have adequate time to rearrange in a compact and short-range inter-related nodular structure. Moreover, the stretching force along the axial direction orients the polymer chains to further decrease free volume on the shell side. The effects of the moisture-induced precipitation and chain orientation are both confined when the air gap is reduced during fabrication.

Table 1
Range of various operating conditions tested and final values

	Range tested	Final values
Dope composition	n/a	PBI, DMAc, PVP, IPA
Dope flow rate (mL/min)	0.9–2.0	0.9
Bore composition	IPA, DMAc, Gly, MeOH, water	IPA
Bore fluid flow rate (mL/min)	0.2–1.0	0.35
Air gap (cm)	0–1.27	0
Winding speed (m/min)	n/a	4.0

Therefore, a small air gap may produce HFMs with a large average pore size (or free volume). As shown in Table 2, no dramatic improvement in pure water flux was observed when the air gap was decreased from 0.5 inch (0.27 cm) to 0.25 inch (0.635 cm), probably because the air gap variation was not significant. To further enhance the HFM water permeability, we adopted a wet spinning technology (i.e., 0 cm air gap). The extruded fibers were instantly immersed into a nonsolvent for a vigorous and rapid phase inversion, in which the polymer chains contract suddenly and create more free volume in the barrier layer. The SEM images show no large open pores a on the surfaces of HFMs fabricated by dry-jet wet spinning (Fig. 3A and B); however, in HFMs prepared by wet spinning, large open pores (50–100 nm) are visible on the shell (Fig. 3C). The extremely large pure water flux (Table 2) indicates the barrier layer density of wet-spun PBI HFMs is much lower than that of the dry-jet wet-spun HFMs.

Table 2
Effect of air-gap on pure water flux at 20 psi

Air gap (cm)	Pure water flux (LMH)	Air gap (inch)	Bore flow rate (cc/min)	Dope flow rate (cc/min)
1.27	4.23	0.5	0.35	0.9
0.635	5.23	0.25	0.35	0.9
0	58	0	0.35	0.9

3.1.2. Optimization of lumen open pore size

The pore size on the lumen side is mainly determined by the bore solution composition and formation of the porous morphology in the lumen during the wet spinning process. Flexible polymer chains extend well in a strong solvent and contract severely in nonsolvents, which reduces the Gibb's free energy. The chain contracting rate is correlated to the interaction between solvent and nonsolvent and affinity of the polymer and nonsolvent [29]. The sponge-like structure next to lumen side is formed by delayed phase inversion, which is also affected by the bore solution composition. The PBI HFMs used in high-pressure filtration process (e.g., NF and RO) have a comparatively low porosity sublayer and a small open pore size on the lumen side that gives them good mechanical strength. However, to produce PBI UF MFMs, a completely different bore solution composition is needed to build a high porosity sublayer and ensure a large open pore size on lumen side for adequate water permeability. We developed an IPA/DMAc/Gly (70/20/10) vol% as the optimized bore solution for RO and NF HFMs in our previous work (Fig. 4A). Gly is a nonsolvent of PBI and it increases the bore solution viscosity and slows the contraction rate of the PBI polymer chain during phase inversion. The lumen side is prone to developing a dense morphology during slow phase inversion because the polymer chains have enough time to rearrange and release free volume. Replacing the Gly with DMAc enlarges the lumen open pore size (Fig. 3B) because DMAc is a strong solvent for PBI. The DMAc-enriched solution is also frequently used as bore solutions for fabrication of NF/RO HFMs [28,30] because DMAc reduces the interaction between bore and dope solutions and slows the coagulation process. When we used pure IPA, the open pore size on lumen side was further enlarged (Fig. 4C). We used these series of experiments to settle on IPA as the bore solution for the final spinning conditions.

3.1.3. Effect of bore solution flow rate on physical dimensions

The RO/NF HFMs require a thick fiber wall to withstand a high hydraulic pressure (200–1,000 psi), but thinner UF HFMs to enhance water permeability at lower operating pressures (<100 psi). According Chung et al.'s [31] mathematical model, the outer diameter/inner diameter ratio (OD/ID) is determined by the flow rate ratio of dope and bore solutions, and the wall thickness can be effectively adjusted by varying the bore solution flow rate with a constant flow rate of dope solution. As shown in Fig. 5, HFM wall thickness gradually decreased from 105 to 89 μm when the bore solution flow rate was increased from 0.3 to 0.4 mL/min. When the bore solution was above 0.4 mL/min, the UF test failed due to the fiber fracture. We used this series of experiments to settle on a bore solution flow rate of 0.35 mL/min as a final spinning condition.

3.1.4. Optimization of the sublayer permeability by introducing macrovoids

Water is a nonsolvent often used to form finger-like macrovoids in PBI HFM fabrication [28,30]. With a nonsolvent, the phase separation pathway of nucleation and growth results in rapid coagulation that usually leads to high-porosity morphology. Water is a stronger nonsolvent than IPA, and its interaction with PBI dope is intense enough to form a larger pore size. However, the SEM images (Fig. 6) indicate the surface morphology on the water side was dense and allowed extremely low

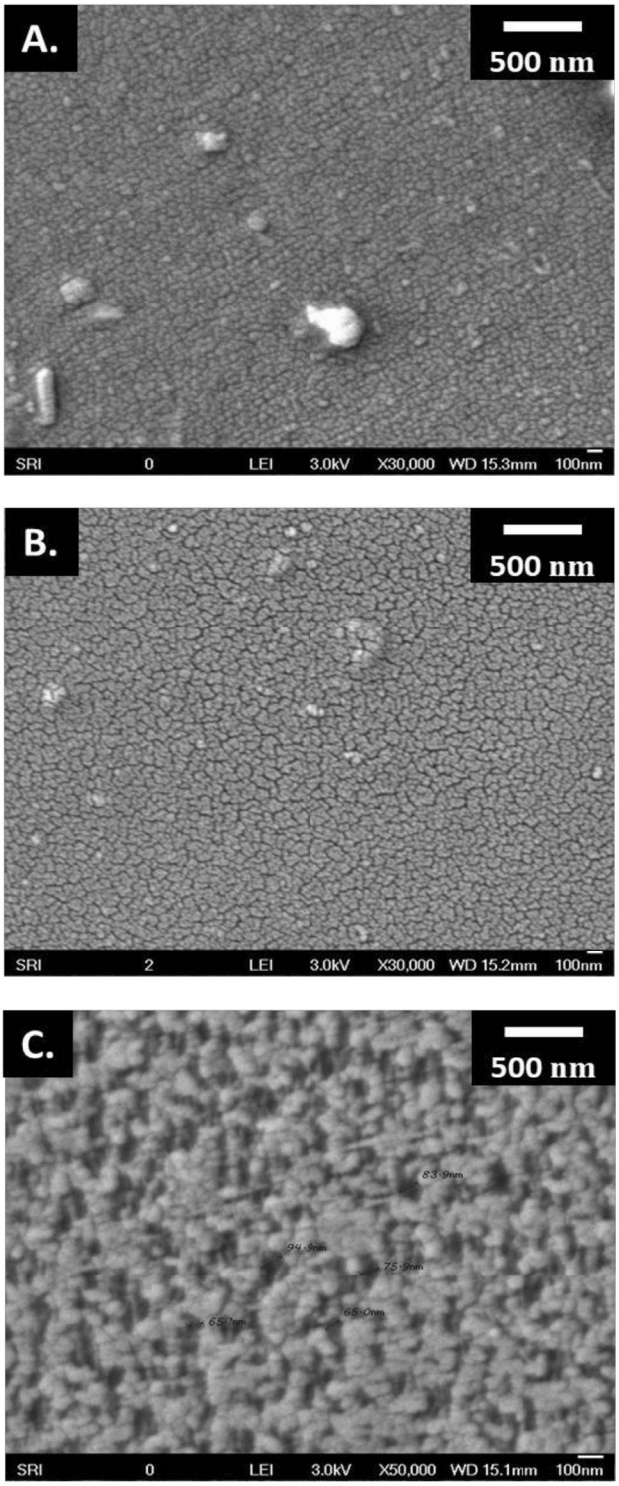

Fig. 3. SEM images of PBI HFM barrier layer surfaces fabricated with air gaps of (A) 0.5 inch (1.27 cm), (B) 0.25 inch (0.635 cm), and (C) 0 inch.

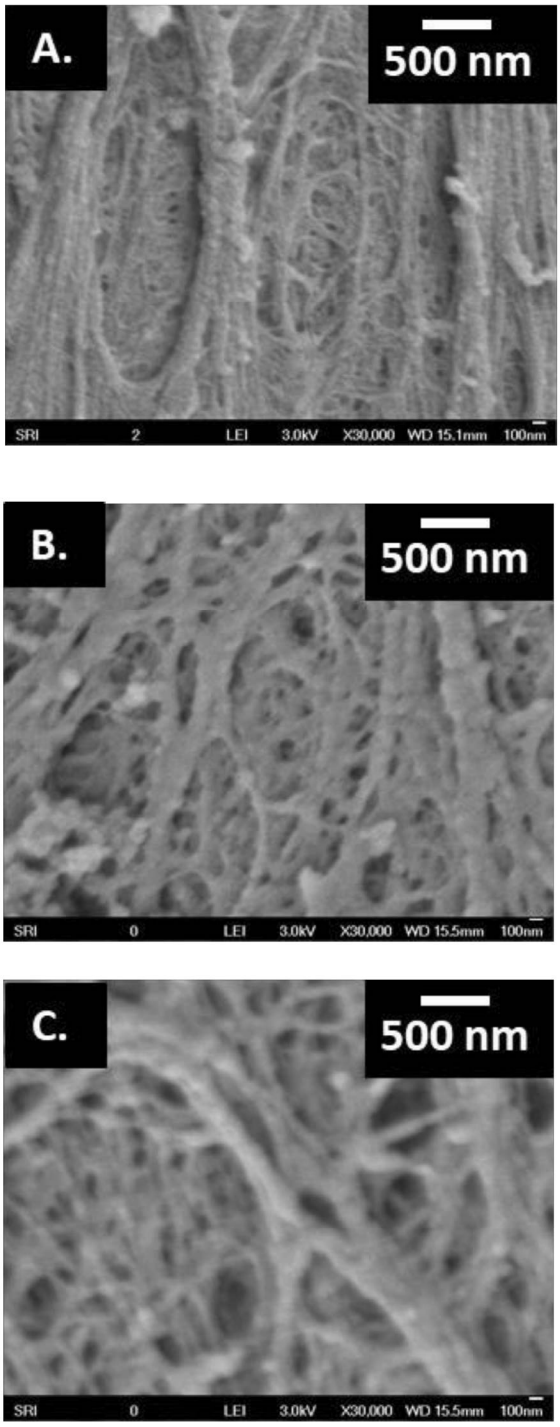

Fig. 4. Lumen pore morphology affected by bore solutions consisting of (A) 70% IPA/20% DMAc/10% Gly, (B) 70% IPA/30% DMAc, and (C) 100% IPA. The coagulation strength of the non-solvent increases from top to bottom, corresponding to increasing lumen pore size from top to bottom.

pure water flux (i.e., 0.25 and 0.37 LMH) aligned with the SEM images. Thus, the water-induced coagulation likely followed a completely different pathway known as spinodal decomposition. Although the process may be induced by a thermal gradient [32], polyethersulfone (PES) [33], and PBI [29] HFM fabrication have resulted in finger-like structures formed by spinodal decomposition due to unbalanced localized stresses from surface tension,

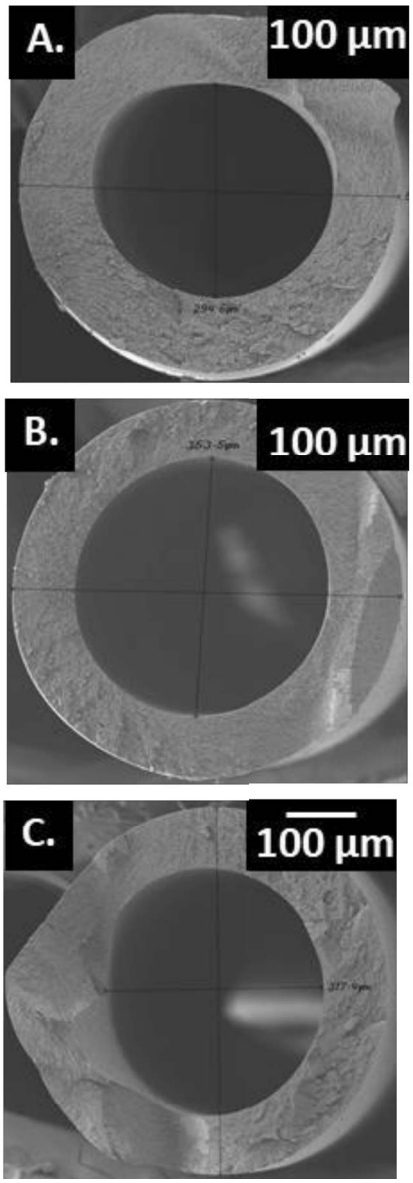

Fig. 5. PBI HFM wall thickness varied by bore solution flow rates: (A) 0.3 mL/min, (B) 0.35 mL/min, and (C) 0.4 mL/min and corresponded to wall thicknesses of (A) 105 µm, (B) 95 µm, and (C) 89 µm, respectively. All membranes had an air gap of 0 cm, dope solution flow rate of 0.9 mL/min, and bore solution of IPA.

solvent-coagulant agglomeration, and radial convective flows of the internal and external coagulants. Since the introduction of macrovoids is always coupled with a dense skin layer on water side, the water-induced phase inversion is not suitable for the fabrication of PBI UF HFMs.

3.1.5. Pore size distribution of the optimized PBI UF HFMs

As aforementioned, the optimized PBI UF HFMs were fabricated with an air gap of 0 cm, a bore solution (pure IPA) flow rate of 0.35 mL/min, and a dope solution flow rate of 0.9 mL/min. Pure water flux of the resulting UF HFMs at 20 psi is as high as 58 LMH. For the capillary flow porometry, gas flow of sample HFM is measured as a function of pressure in dry and wet states, respectively (Fig. 7). When the membrane is filled by liquid, the largest pores are emptied at a certain threshold leading to a significant gas flow increment. The smaller pores are opened with the further increment of pressure. According to the Laplace equation, the smallest pores are completely opened when the "Dry" and "Wet" curves are overlapped [34]. The optimized PBI UF HFMs have pore size distributed in 21–25 nm range and a mean pore size of 22 nm (Fig. 8); analysis summary is provided in the Supplemental data.

3.2. Filtration tests with humic acid, bovine serum albumin, and bentonite

Fouling limits long-term membrane filtration processes and contributes to decay of membrane permeability. Fouled surfaces require maintenance and cleaning, which can be expensive. Foulants are briefly classified into four categories: macromolecules, biological substances, particulates, and ions [35]. The first three are regarded as the main causes of UF fouling, and we studied HA, BSA, and bentonite clay, respectively, as we evaluated the anti-fouling capability of the newly developed PBI UF HFM. All membranes used in filtration tests had the final spinning conditions of: air gap = 0 cm, bore flow rate = 0.35 mL/min, dope flow rate of 0.9 mL/min, and a bore solution of IPA (Table 1).

Humic acid consists of anionic hydrophobic macromolecules with a wide molecular weight distribution and is well known as natural organic matter (NOM) that contributes to unpleasant odors and tastes in water [36]. The causes of HA fouling are attributed to two mechanisms, pore absorption [37], and gel/cake layer formation [38]. Pore adsorption occurs due to specific interactions (e.g., van der Waals forces, electrostatic attraction, or chemical bonding) between solutes and the membrane. The interaction between PBI and HA is thought to result from van der Waals forces that are enhanced by the hydrophobic–hydrophobic effect. The effect occurs spontaneously and rapidly, and instant flux decreases are apparent in all curves in Fig. 9. Gel/cake layer formation is caused by concentration polarization and consolidation of highly concentrated HA solution in the immediate vicinity of the membrane surface. The HFMs exhibited a slight decrease (10%–15%) in flux over time during a 3 h filtration test. A low pH confines the deprotonation of acidic functional groups in HA and reduces electrostatic repulsion between HA molecules. Thus, HA gel layer formation is promoted in acidic circumstances, resulting in much lower flux than in neutral or basic solutions [36]. However, the gel layer formation takes time and the significantly lower initial flux at pH 3.84 is probably due to pore size reduction induced by protonation of the secondary amine groups in PBI molecules; this was also observed in our previous study [5].

Native (non-aggregated) proteins typically have complex molecular structures with multiple charge points that result in an extremely complicated fouling process. To simplify the fouling process, BSA solution was prepared in a phosphate buffer with a pH value (7.4) higher than the isoelectric point of BSA (pH = 4.7 [39]). Therefore, BSA in the feed solution contained negative charges, and the resulting fouling process was comparable to that of HA. Following a

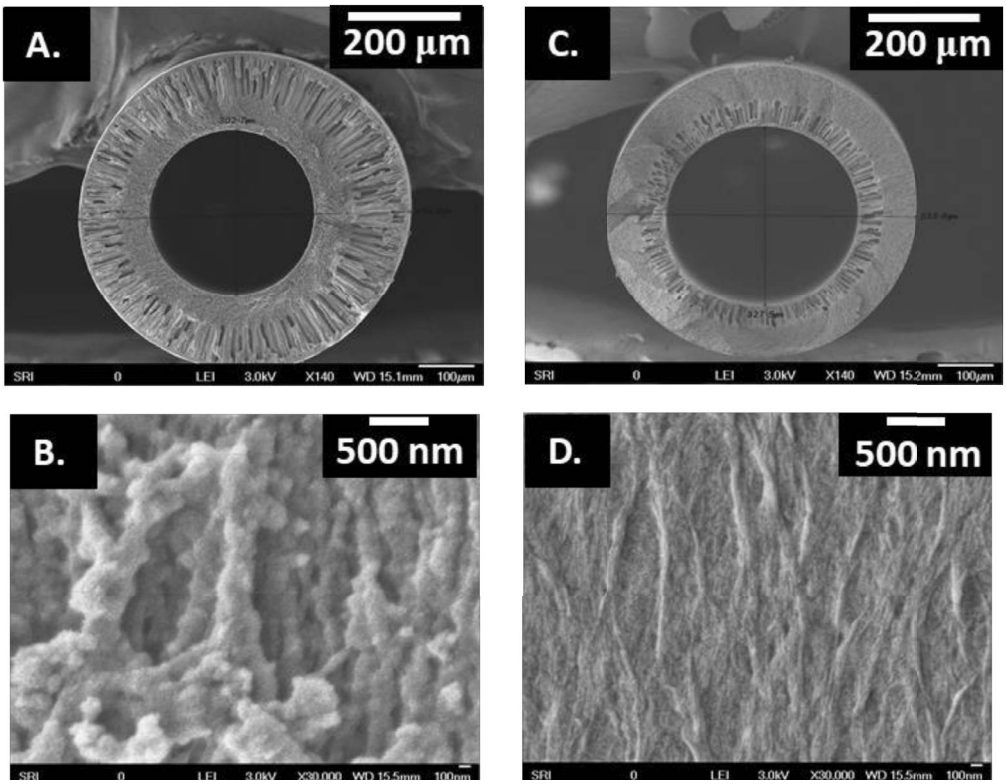

Fig. 6. SEM images of membrane morphology with water as the coagulation bath on the (left column, A and B) produced a pure water flux of 0.25 LMH, and water as the bore solution (right column, C and D) produced a pure water flux of 0.37 LHM. Panels (A and C) show the overall cross section. Panels (B and C) show the lumen surface.

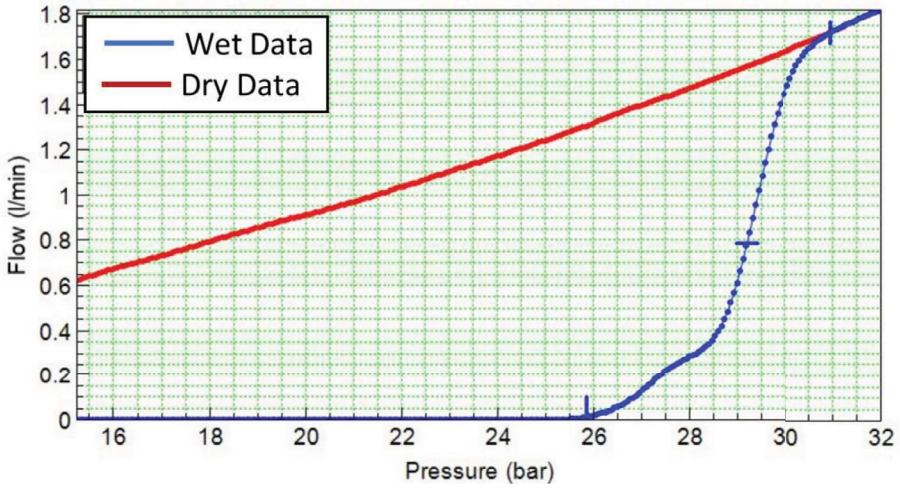

Fig. 7. Gas flow rate as a function of pressure for "Wet" and "Dry" runs.

3 h test, the PBI HFMs exhibited only a slight flux decrease (<10%) (Fig. 10).

The bentonite particulates are rigid and the fouling process is a function of the cake formation process, in which particles build up layer by layer on the HFM surface and lead to additional resistance to the permeate flow [40]. When the feed solution had turbidity of 70 NTU, the flux remained constant over the 3 h test (Fig. 11).

4. Conclusions

We prepared PBI UF HFMs with an open pore surface size of 50–100 nm using a wet-spinning process. To control the resistance to water flow in sublayer, we used 100 vol% IPA as a bore solution to maximize the open pore size on lumen side. The flow rate ratio of bore and dope solutions was increased to 9:4 for a fiber wall as thin as 89 µm. The resulting UF HFMs exhibited pore size in 21–25 nm

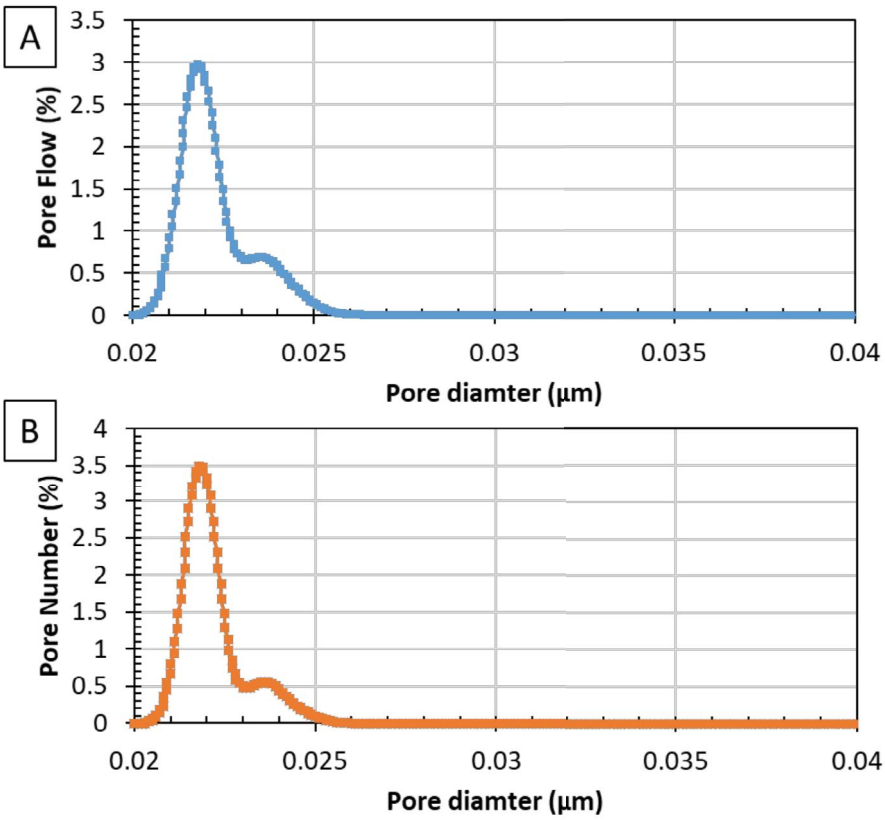

Fig. 8. Shows pore size distributed in 21–25 nm range and a mean pore size of 22 nm for both: (A) differential percent flow vs. pore size, and (B) differential pore number percent area vs. pore size.

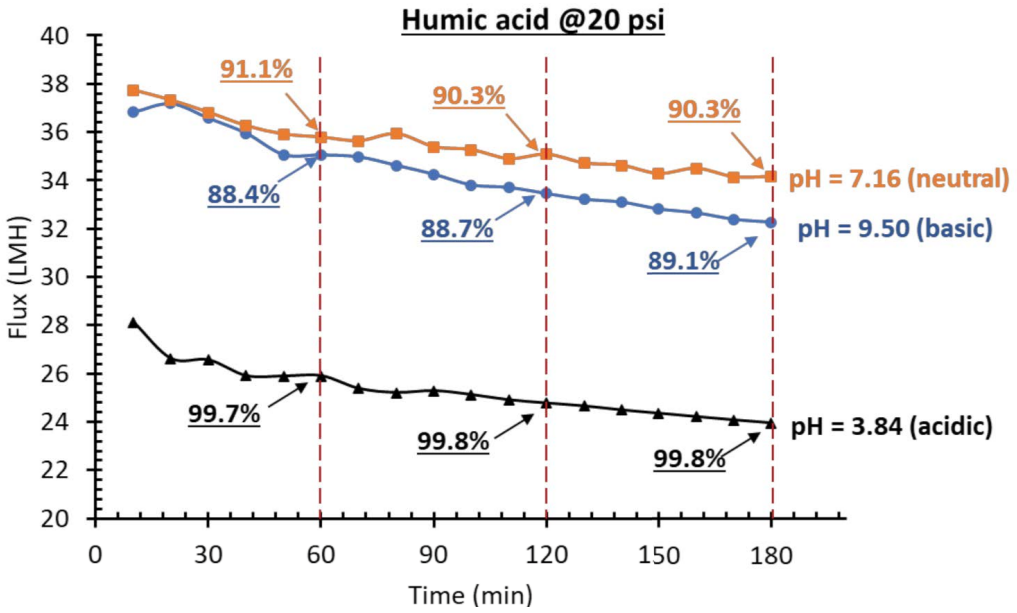

Fig. 9. Humic acid results at acid, basic, and neutral pH values. The flux order showed neutral > basic > acid. Additionally, the %rejection at 60, 120, and 180 min intervals are shown for all pH values. The acid condition showed nearly complete rejection, while the basic and neutral conditions ranged from 88% to 91%rejection.

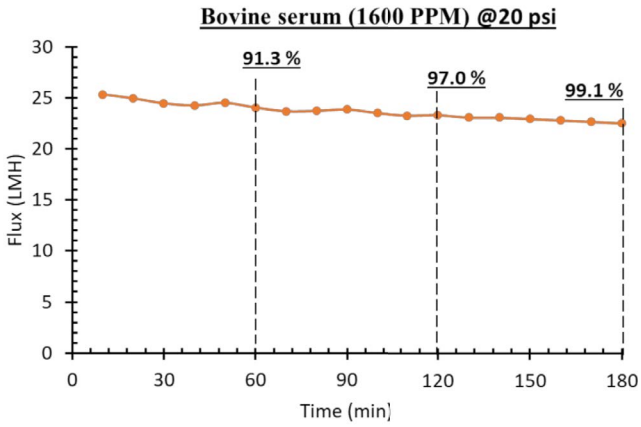

Fig. 10. Bovine serum albumin results displayed a relatively constant flux (<10% decrease) over the 3 h experiment with a >99% %rejection over the duration of the experiment.

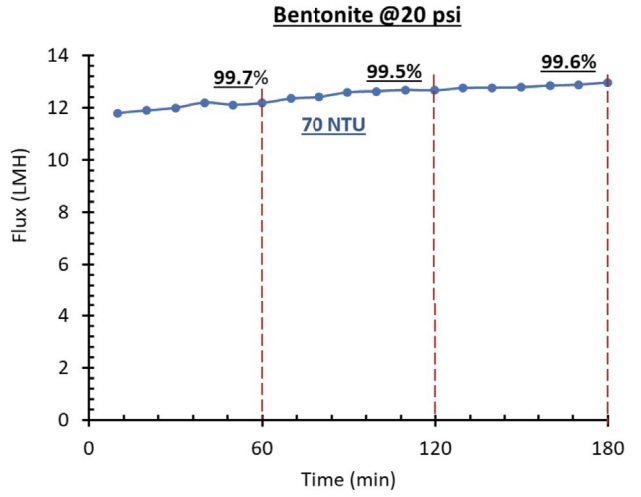

Fig. 11. At a turbidity of 70 NTU, the membrane maintained a stable flux close to its pure water value and had a >99% rejection rate.

and an optimal pure water flux up to 58 LMH at 20 psi. This breakthrough enabled us to use SRI's versatile fiber spinning line to fabricate PBI HFMs for various applications (e.g., gas separation, NF, RO, and UF) by varying key spinning factors, such as air gap, solution composition, and solution flow rate. The PBI UF HFMs had good antifouling properties. In a 3 h filtration test, there was no fouling in a 70 NTU bentonite suspension, <10% flux reduction in a 1,500–1,600 ppm BSA solution, and a 10%–15% flux decrease in a 50 mg/L HA solution at different pH values.

Funding

This research was funded by King Abdulaziz City for Science and Technology (KACST), the KACST SRI International project number is P24747.

Acknowledgments

The authors wish to acknowledge the financial support for the current development from the KACST, Riyadh and Greg Copeland, and Mike Gruender of the PBI Performance Products, Inc. for their continued support in participating in PBI product development projects at SRI.

References

[1] D.S. Sholl, R.P. Lively, Seven chemical separations to change the world, Nature, 532 (2016) 435–437.
[2] T. Turken, R.S. Tasdemir, E.A. Genceli, V.V. Tarabara, I. Koyuncu, Progress on reinforced braided hollow fiber membranes in separation technologies: a review, J. Water Process Eng., 32 (2019) 100938, doi: 10.1016/j.jwpe.2019.100938.
[3] C.F. Wan, T. Yang, G.G. Lipscomb, D.J. Stookey, T.S. Chung, Design and fabrication of hollow fiber membrane modules, J. Memb. Sci., 538 (2017) 96–107.
[4] X. Yang, R. Wang, A.G. Fane, C.Y. Tang, I.G. Wenten, Membrane module design and dynamic shear-induced techniques to enhance liquid separation by hollow fiber modules: a review, Desal. Water Treat., 51 (2013) 3604–3627.
[5] X. Wang, P. Jayaweera, R.A. Alrasheed, S.A. Aljlil, Y.M. Alyousef, M. Alsubaei, H. AlRomaih, I. Jayaweera, Preparation of polybenzimidazole hollow-fiber membranes for reverse osmosis and nanofiltration by changing the spinning air gap, Membranes, 8 (2018) 113, doi: 10.3390/membranes8040113.
[6] G. Krishnan, I. Jayaweera, A. Sanjrujo, K. O'Brien, R. Callahan, K. Berchtold, D.-L. Roberts, W. Johnson, Fabrication and Scale-up of Polybenzimidazole (PBI) Membrane Based System for Precombustion-Based Capture of Carbon Dioxide, Los Alamos National Lab.(LANL), Los Alamos NM, 2013.
[7] K.Y. Wang, Y. Xiao, T.S. Chung, Chemically modified polybenzimidazole nanofiltration membrane for the separation of electrolytes and cephalexin, Chem. Eng. Sci., 61 (2006) 5807–5817.
[8] T.S. Chung, A critical review of polybenzimidazoles: historical development and future R&D, J. Macromol. Sci., Part C Polym. Rev., 37 (1997) 277–301.
[9] A.A. Tashvigh T.S. Chung, Facile fabrication of solvent resistant thin film composite membranes by interfacial crosslinking reaction between polyethylenimine and dibromo-p-xylene on polybenzimidazole substrates, J. Membr. Sci., 560 (2018) 115–124.
[10] H. Thiess, M. Leuthold, U. Grummert, J. Strube, Module design for ultrafiltration in biotechnology: hydraulic analysis and statistical modeling, J. Membr. Sci., 540 (2017) 440–453.
[11] A.V Bildyukevich, T.V Plisko, F. Lipnizki, S.A. Pratsenko, Correlation between membrane surface properties, polymer nature and fouling in skim milk ultrafiltration, Colloids Surf., A, 605 (2020) 125387, doi: 10.1016/j.colsurfa.2020.125387.
[12] D.A. Musale, S.S. Kulkarni, Relative rates of protein transmission through poly (acrylonitrile) based ultrafiltration membranes, J. Membr. Sci., 136 (1997) 13–23.
[13] R. Ghosh, Z.F. Cui, Protein purification by ultrafiltration with pre-treated membrane, J. Membr. Sci., 167 (2000) 47–53.
[14] S. Simone, F. Galiano, M. Faccini, M. Boerrigter, C. Chaumette, E. Drioli, A. Figoli, Preparation and characterization of polymeric-hybrid PES/TiO_2 hollow fiber membranes for potential applications in water treatment, Fibers, 5 (2017) 14, doi: 10.3390/fib5020014.
[15] I. Jayaweera, P. Jayaweera, S. Bhamidi, R. Elmore, E. Perea, X. Wang, Development of a Pre-combustion CO_2 Capture Process Using High-Temperature PBI Hollow-Fiber Membranes, 14th Greenhouse Gas Control Technologies Conference, Melbourne, 2018, pp. 21–26.
[16] G.C. Kapantaidakis, G.H. Koops, High flux polyethersulfone-polyimide blend hollow fiber membranes for gas separation, J. Membr. Sci., 204 (2002) 153–171.
[17] S.S. Hosseini, N. Peng, T.S. Chung, Gas separation membranes developed through integration of polymer blending and

dual-layer hollow fiber spinning process for hydrogen and natural gas enrichments, J. Membr. Sci., 349 (2010) 156–166.
[18] F.S. Model, L.A. Lee, PBI Reverse Osmosis Membranes: An Initial Survey, H.K. Lonsdale, H.E. Podall, Eds., Reverse Osmosis Membrane Research, Springer, Boston MA, 1972, pp. 285–297.
[19] L.C. Sawyer, R.S. Jones, Observations on the structure of first generation polybenzimidazole reverse osmosis membranes, J. Membr. Sci., 20 (1984) 147–166.
[20] K.Y. Wang, Q. Yang, T.S. Chung, R. Rajagopalan, Enhanced forward osmosis from chemically modified polybenzimidazole (PBI) nanofiltration hollow fiber membranes with a thin wall, Chem. Eng. Sci., 64 (2009) 1577–1584.
[21] G.R. Guillen, Y. Pan, M. Li, E.M.V. Hoek, Preparation and characterization of membranes formed by nonsolvent induced phase separation: a review, Ind. Eng. Chem. Res., 50 (2011) 3798–3817.
[22] I. Jayaweera, G.N. Krishnan, A. Sanjurjo, P. Jayaweera, S. Bhamidi, Process for Fabricating PBI Hollow Fiber Asymmetric Membranes for Gas Separation and Liquid Separation, Google Patents, 2016.
[23] J. Lowe, M.M. Hossain, Application of ultrafiltration membranes for removal of humic acid from drinking water, Desalination, 218 (2008) 343–354.
[24] Y. Chen, W. Xu, H. Zhu, D. Wei, F. He, D. Wang, B. Du, Q. Wei, Effect of turbidity on micropollutant removal and membrane fouling by MIEX/ultrafiltration hybrid process, Chemosphere, 216 (2019) 488–498.
[25] Y. Marselina, P. Le-Clech, R. Stuetz, V. Chen, Detailed characterisation of fouling deposition and removal on a hollow fibre membrane by direct observation technique, Desalination, 231 (2008) 3–11.
[26] X. Huang, B.T. McVerry, C.M. Jones, M.C.Y. Wong, E.M.V. Hoek, R.B. Kaner, Novel chlorine resistant low-fouling ultrafiltration membrane based on a hydrophilic polyaniline derivative, J. Mater. Chem. A, 3 (2015) 8725–8733.
[27] C.P. Holliday, T.C. Rasmussen, W.P. Miller, Establishing the Relationship Between Turbidity and Total Suspended Sediment Concentration, Proceedings of the 2003 Georgia Water Resources Conference, Georgia, 2003.
[28] K.Y. Wang, T.S. Chung, J.J. Qin, Polybenzimidazole (PBI) nanofiltration hollow fiber membranes applied in forward osmosis process, J. Membr. Sci., 300 (2007) 6–12.
[29] T. Chung, X. Hu, Effect of air-gap distance on the morphology and thermal properties of polyethersulfone hollow fibers, J. Appl. Polym. Sci., 66 (1997) 1067–1077.
[30] K.Y. Wang, T.S. Chung, Fabrication of polybenzimidazole (PBI) nanofiltration hollow fiber membranes for removal of chromate, J. Membr. Sci., 281 (2006) 307–315.
[31] T. Chung, Z. Xu, W. Lin, Fundamental understanding of the effect of air-gap distance on the fabrication of hollow fiber membranes, J. Appl. Polym. Sci., 72 (1999) 379–395.
[32] S.A. McKelvey, W.J. Koros, Phase separation, vitrification, and the manifestation of macrovoids in polymeric asymmetric membranes, J. Membr. Sci., 112 (1996) 29–39.
[33] Z.L. Xu, F.A. Qusay, Polyethersulfone (PES) hollow fiber ultrafiltration membranes prepared by PES/non-solvent/NMP solution, J. Membr. Sci., 233 (2004) 101–111.
[34] M. Mulder, J. Mulder, Basic Principles of Membrane Technology, Springer Science & Business Media, Netherlands, 1996.
[35] X. Shi, G. Tal, N.P. Hankins, V. Gitis, Fouling and cleaning of ultrafiltration membranes: a review, J. Water Process Eng., 1 (2014) 121–138.
[36] W. Yuan, A.L. Zydney, Humic acid fouling during ultrafiltration, Environ. Sci. Technol., 34 (2000) 5043–5050.
[37] K.L. Jones, C.R. O'Melia, Protein and humic acid adsorption onto hydrophilic membrane surfaces: effects of pH and ionic strength, J. Membr. Sci., 165 (2000) 31–46.
[38] A.E. Childress, S.S. Deshmukh, Effect of humic substances and anionic surfactants on the surface charge and performance of reverse osmosis membranes, Desalination, 118 (1998) 167–174.
[39] J. Hu, S. Li, B. Liu, Adsorption of BSA onto sulfonated microspheres, Biochem. Eng. J., 23 (2005) 259–263.
[40] P. Bacchin, P. Aimar, V. Sanchez, Model for colloidal fouling of membranes, AIChE J., 41 (1995) 368–376.

Supplementary information

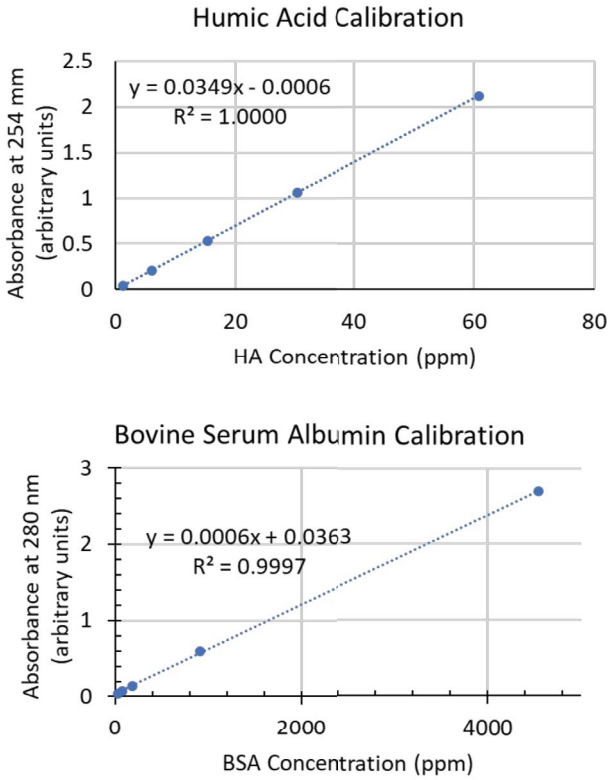

Fig. S1. Calibration curves for humic acid and bovine serum albumin.

Table S1
Quantachrome 3Gwin-pore size analysis summary

Parameter	Value
Maximum pore size	0.0248 µm
Mean flow pore size	0.0219 µm
Minimum pore size	0.0207 µm
Bubble point pressur	25.8491 bar
Bubble point flow rate	0.0123 l/m
Bubble point threshold tolerance	0.01
Fluid density	1,850.0 kg/m³
Fluid temperature	23.00°C
Surface tension	16.00 dyn/cm
Contact angle	0.00°
Shape factor	1
Size factor	0.64
Pore tortuosity	1
Total sample diameter	25.000 mm
Measured sample diameter	20.000 mm
Measured sample area	3.1416 cm²